Molecular Docking of Secondary Metabolites of Marine Macroalgae *Sargassum vulgare* Against Exotoxin A

Najme Baghernezhad[1]*, Bita Archangi[1]*, Ahmad Savari[1], Faedeh Amini[1]

Received: 2024-03-20 Accepted: 2024-05-27

Abstract

Sargassum is described as possessing biological metabolites that exhibit a range of activities including immuno-modulatory, analgesic, antioxidant, neuroprotective, anti-bacterial, anti-inflammatory, anti-tumor, and anti-viral activities to discover the antibacterial activity of the secondary metabolites of *Sargassum vulgare* by in silico approach. Samples were collected from the coastal zone of Boushehr, Persian Gulf. Species identification was performed by morphological and molecular analyses. The ethanolic and methanolic extracts of *S. vulgare* were subjected to GC-MS. The metabolites identified through GC-MS analysis were selected as ligands for interaction with the protein receptor in a molecular docking study using the PyRx software. Subsequently, nine ligands exhibiting high bind affinity and favorable interactions were assessed for their physicochemical, pharmacokinetic, and drug-likeness properties via the SwissADME web server. GC-MS analysis identified the presence total of 28 secondary metabolites comprising 16 ethanolic and 12 methanolic compounds. A docking study of these bioactive compounds showed their binding affinity and reactivity with the exotoxin A of *Pseudomonas aeruginosa*. Based on the ADME results, two compounds, Dioctyl Benzene-1, 2-Dicarboxylate, and Bis (6-Methylheptyl) Benzene-1, 2-Dicarboxylate, exhibited superior properties for drug targeting. The results suggested that the majority of compounds derived from *S. vulgare* extracts were effectively docked at the active site of exotoxin A of *P.aeruginosa*, Therefore, *S. vulgare* may serve as a sources of phytochemical metabolites with antibacterial properties, potentially mitigating the adverse effects associated with synthetic drugs. Further exploration into clinical applications is warranted.

Keywords *Sargassum,* Docking, Exotoxin A, Drug targeting

Introduction

There has been a growing interest of utilizing medicinal herbs recently for the prevention and prevention and treatment of diseases attributed to their low toxicity, minimal side effects, absence

1-Department of Marine Biology, Faculty of Marine Science and Oceanography, Khorramshahr University of Marine Science and Technology, Khorramshahr, Iran.
*Corresponding author email address: email: b.archangi@kmsu.ac.ir
Doi: 10.48308/JPR.2024.235599.1078

of drug resistance, limited drug residues, and affordability (Liao et al., 2022). Macroalgae are known to contain a diverse array of bioactive metabolites, including polysaccharides, alkaloids, organic acids, flavonoids, and phenols, which possess pharmacological properties that include antibacterial and antiviral, as well as enhancement of the immune system and body's capacity to combat infections (Liao et al., 2022). The incidence of antibiotic-resistant bacteria poses a significant challenge in healthcare, necessitating the exploration of alternatives to conventional antibiotics, and chemical drugs. Studies on the application of secondary metabolites derived from natural sources as substitutes for chemical antibiotics has been on the rise (Silva et al., 2020). According to the studies, brown algae, particularly *Sargassum*, exhibit bioactive properties effective against various gram-negative and gram-positive bacteria, including *Escherichia coli*, *Pseudomonas aeruginosa*, *Clostridium perfringens*, *Staphylococcus aureus*, etc. (Arguelles et al., 2019). Consequently, *Sargassum* is regarded as a promising sustainable natural resource with antibacterial properties related to its secondary metabolites.

P. aeruginosa synthesizes a variety of extracellular toxins, including pigments, phytotoxic agents, phospholipases, hydrocyanic acids, proteolytic enzymes, enterotoxins, and exotoxins. The primary determinant of the pathogenicity of *P. aeruginosa* is its ability to produce exotoxins. These exotoxins are responsible for a range of severe health issues, including leukopenia, acidosis, circulatory collapse, liver necrosis, pulmonary edema, hemorrhage, and tubular necrosis of the kidneys (Liu, 1974). Exotoxin A (ETA) produced by *P. aeruginosa* serves as a virulence factor that is secreted in response to low environmental iron levels. The protein consists of three distinct domains and comprises 613 amino acid residues. Analysis of the modular domain structure of the toxin revealed that domain I (amino acids 1 to 252 (Ia) and 365 to 395 (Ib)) is associated with receptor binding, domain II (aa 253 to 364) plays a role in transmembrane targeting, and domain III (amino acids 396 to 613) is linked to the enzymatic fuction of ETA, specifically as an ADP-ribosyl transferase (Wedekind et al., 2001). *P. aeruginosa* exhibited significant toxicity towards eukaryotic cells, leading to the cessation of protein synthesis. This effect is performed through enzymatic ADP-ribosylation of a specific post-translationally modified histidine residue in eEF-2 known as diphthamide (Wedekind et al., 2001).

Virtual screening has significantly enhanced the prospects for researchers to identify new marine natural products (Prasanth and Suresh Kumar, 2020). Molecular docking-based virtual screening serves as a computational method in drug design, facilitating the discovery process by reducing both time and costs. This docking technique focusing on analyzing ligand-receptor interactions, relying on a scoring function that estimates the binding affinity of the ligands to receptors (Gade et al., 2023). The primary aim of molecular docking is to establish a ligand-receptor complex that exhibit an optimized conformation and minimized binding free energy (Teibo et al., 2021).

In the present study, the bioactive compounds of *S. vulgare* were subjected to molecular docking against the ETA of *P. aeruginosa*, to evaluating the binding affinity and interaction potential of these compounds for antibiotic drug targeting as .

Material and methods

sampling and preparation

Samples of *S. vulgare* were collected from the intertidal region of Boushehr, Persian Gulf (28°54'49"N 50°48'46"E), during April 2022. The identification of the *S. vulgare* species was conducted through molecular and morphological analyses, utilizing established identification keys (Guiry et al., 2014).

The collected samples weighing 5 kg, were washed with seawater to eliminate sand particles and any necrotic components. Subsequently, these samples were transported, where they were rinsed with tap water to remove surface salts followed by a washwith sterilized distilled water. The samples were then air-dried at room temperature until they were completely dry. Finally, the dried ere ground using a grinder and stored in a sterilized bag in preparation for extraction (Faisal al-hashdy et al., 2022).

Preparation of S. vulgare extract

A 25 g portion of the powdered *S. vulgare* sample was enclosed in Whatman filter paper, and both ethanolic and methanolic extractions were performed (250 ml, 1:10 w/v) separately, yielding a colorless solution via a Soxhlet apparatus. The extract was then filtered by Whatman No. 1 filter paper, concentrated at the temperature range of 40-50 °C using a rotary evaporator, and subsequently dried at 40 °C in a hot air oven. The resulting dark, viscous solid was utilized for the subsequent stage (Rajkumar et al., 2018).

Gas chromatography-mass spectrophotometry (GC-MS) analysis

The extracts of *S. vulgare* were subjected to GC-MS analysos using a Gas Chromatography-Mass Spectrometry with an Agilent 7890A gas chromatogram and an Agilent 5975 mass spectrometer, both from USA). The system was equipped with an HP-5 MS fused silica column comprising

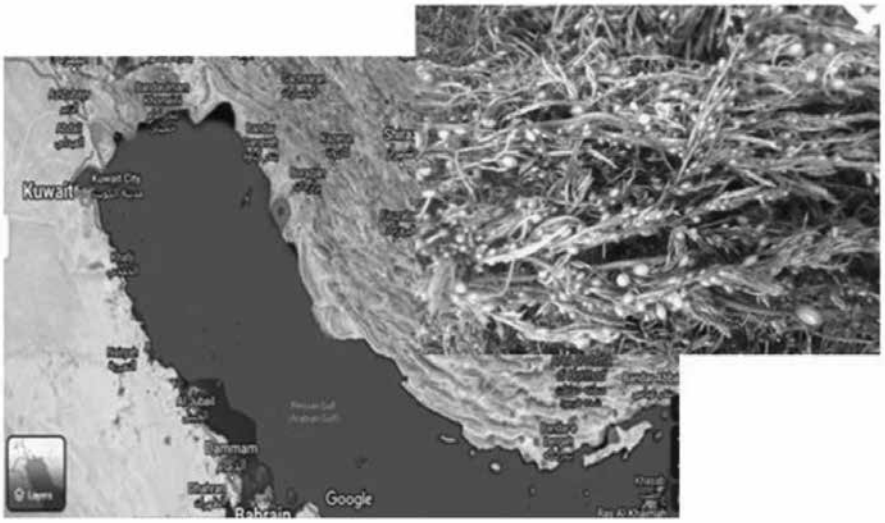

Fig. 1. Collection site of S.vulgare in the coastal zone of Boushehr, Persian Gulf

5% phenyl and 95% dimethyl polysiloxane, measuring 30.0 m × 0.25 mm, with a film thickness 0.25 µm. Helium served as the carrier gas, set to a column flow rate of 1.0 ml/min. The injector operated in split mode with a split ratio of 1:50, and the injection temperature was maintained at 280 °C. The temperature program for the oven commenced at 40 °C for 1 minute, increasing at the rate of 5° C/min until reaching to 300 °C, where it remained for 3 minutes. The transfer line temperature was set at 280 °C and the total run time was 56 minutes. The identification of secondary phytochemical components in each *S. vulgare* extract was achieved by comparing their retention times and mass spectra against the WILEY7n.l and NIST08.L mass spectral database (Abu Ahmed et al., 2021).

Molecular docking

Receptor and ligand preparation

The current study was designed to screen phytochemicals derived from *S. vulgare* virtually to identify the inhibitory effect against the ETA. The three-dimensional structure complex of the ETA protein (PDB ID: 1IKQ at 1.62 Å) was retrieved from the RCSB Protein Data Bank in PDB format, serving as the receptor. The metabolites of the brown algae *S. vulgare, acquired* through GC-MS analysis and utilized as ligand input structures, were sourced from the PubChem database in SDF format (Table 1 and Table 2) (Prasanth and Suresh Kumar, 2020).

For the docking procedure, the ligands and target protein were initially prepared by OpenBabel online converter and UCSF Chimera 1.11, respectively (Adetayo and Anyasor, 2022). The SDF file of the ligands was transformed into PDB format using openBabel (Bultum et al., 2022). Subsequently, hydrogen atoms were added, hydrogen bonding was optimized, and all the atomic clashes were removed through structure minimization. The energy minimization of the protein was performed for 1000 steps, and non-essential ligands, including water molecules, were eliminated to enhance the docking outcomes. Then both ligands and the protein were transferred to the PyRx tool for the molecular docking analysis (Miandad et al., 2022).

Docking by the PyRx

In silico molecular docking was utilized to predict the interactions between ETA and phytochemical ligands, focusing on their conformations and binding free energies (kcal/mol). This research employed AutoDock Vina, recognized as the premier bioinformatics tool for docking (Bultum et al., 2022). The prepared protein and ligands were imported into the PyRx software, where docking was performed by Vina mode (Garg et al., 2020). The PDB files for both the ligands and protein were converted to PDBQT format via PyRx to ensure compatibility with Vina (Haddad et al., 2022). Multiple ligands were selected against the receptor using PyRx multiple ligands have been selected against the receptor (Garg et al., 2020). Prior to executing Vina, a grid box measuring 28 × 25× 24 Å was established on the receptor ‘s surface, with the catalytic residues designated as the centers of the grid box (Mohammed et al., 2022). The results of the docking were analyzed to identify the lowest binding affinity and the nature of interactions

(Kothandan et al., 2021). PyMOL was employed to visualize the binding pose of the docked protein-ligand complex and to convert the output from PDBQT format to PDB format. Subsequently, the PDB format of the docked target protein-ligand complex was analyzed using BIOVIA Discovery Studio, which illustrated the binding sites interactions between the receptor and the docked ligand (Bultum et al., 2022). LigPlot Version V.2.2.8 was utilized to depict protein-ligand interactions in a schematic 2D representation (Mishra and Dey, 2019). Moreover, all interactions between the target protein and the ligand were visualized using the Protein-Ligand Interaction Profiler (PLIP) webserver (Bultum et al., 2022).

ADME studies of ligands with top binding scores

The evaluation of the absorption, distribution, metabolism, and excretion (ADME) of the leading binding ligands was done by the SwissADME web server (http://www.swissadme.ch/). The analysis utilized the canonical SMILES representations of the top ligands, yielding outputs that encompassed physicochemical parameters, pharmacokinetic properties, and drug-likeness assessments (Praveen et al., 2023). The physicochemical descriptors obtained included molecular weight (MV), the count of heavy atoms, the number of hydrogen bond acceptor and donor, molar refractivity (MR), topological polar surface area (TPSA), and solubility, among other relevant parameters. Pharmacokinetic properties like gastrointestinal (GI) absorption and blood-brain barrier (BBB) permeability were evaluated. The drug-likeness properties were analyzed through the application of the Lipinski and Veber Rule. Finally, the BOILED-Egg plot (Brain Or IntestinaL EstimateD permeation) was employed to illustrate the capacity of compounds to traverse the blood-brain barrier and their absorption through the human gastrointestinal tract (Daina et al., 2017; Praveen et al., 2023).

Results

The GC-MS analysis of S. vulgare

The analysis of extracts via GC-MS was done following standard protocols utilizing the Agilent Gas Chromatography–Mass Spectrometry system. The mass spectra of the identified compounds were compared against databases from the National Institute of Standards and Technology (NIST) and the WILEY online library. The chromatograms depicting the metabolites of *S. vulgare* are presented in Figures 2 and 3. The GC-MS evaluations of the ethanolic and methanolic extracts of *S. vulgare* indicated the presence of 28 secondary metabolites, comprising 16 compounds from the ethanolic extract (as detailed in Table 1), and 12 compounds from methanolic extract (as outlined in Table 2). The chemical structures and CID codes are sourced from PubChem.

Molecular docking

The bioactive compounds identified through GC-MS analysis were docked at the binding site of the ETA protein of *P. aeruginosa* using Autodock vina (Mohammed et al., 2022). The selection of binding sites was initially based on UniProt report and a comprehensive literature review concerning the target protein 1IKQ.The known catalytic

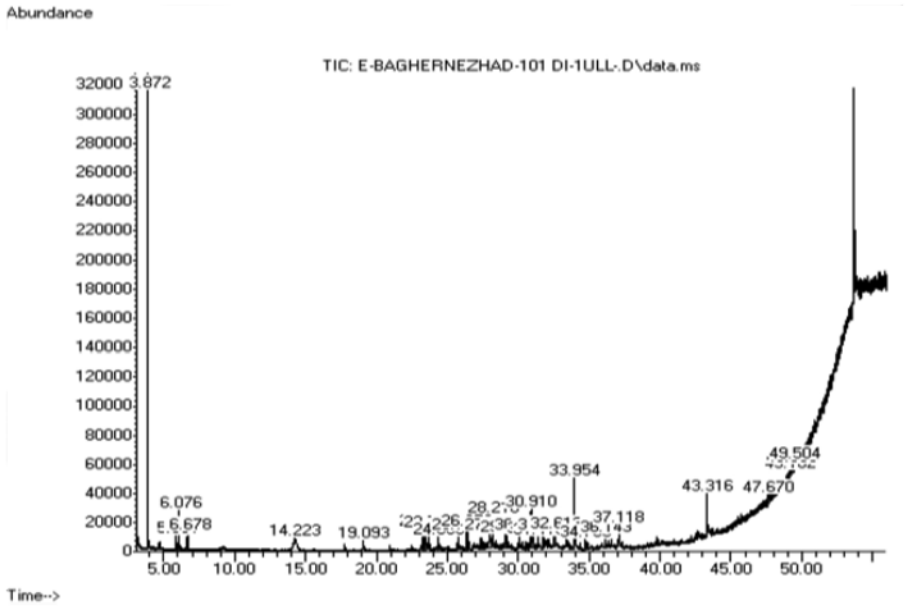

Fig. 2. GC-MS chromatogram of the Ethanolic extract of *S. vulgare*

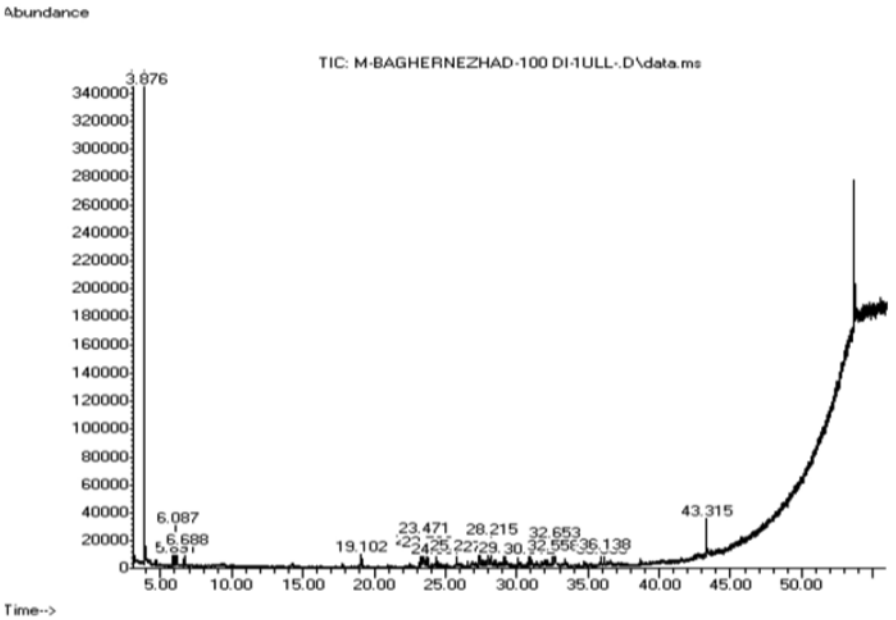

Fig. 3. GC-MS chromatogram of the methanolic extract of *S. vulgare*

Table 1. Secondary phytochemical compounds identified by GC-MS in ethanolic extracts of *S. vulgare*

Peak RT	Area %	Secondary compounds	CID	Qual	Molecular formula	Chemical structure
28.21	3.56	1-Iodotridecane	545617	78	$C_{13}H_{27}I$	
23.72	2.11	2,4-ditert-butylphenol	7311	72	$C_{14}H_{22}O$	
24.38	1.49	3,5dimethyloctan-2-one	537874	72	$C_{10}H_{20}O$	
25.75	2.34	Tridecan-3-yl 2-methoxyacetate	542291	72	$C_{16}H_{32}O_3$	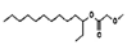
27.98	3.55	Octadecane	11635	72	$C_{18}H_{38}$	
33.95	7.65	ethyl hexadecanoate	12366	98	$C_{18}H_{36}O_2$	
32.61	1.42	9-Octylicosane	280905	64	$C28H_{58}$	
33.95	2.45	Hentriacontane	12410	68	$C_{31}H_{64}$	
30.91	4.95	2-[12-(oxiran-2-yl)dodecyl]oxirane	543423	50	$C_{16}H_{30}O_2$	
31.05	1.76	4-Methyldocosane	520181	53	$C_{23}H_{48}$	
31.41	1.42	(E)-1-methoxydodec-2-ene	88030105	35	$C_{13}H_{26O}$	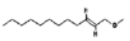
31.77	1.95	2,2,2-trichloroethyl undec-10-enyl carbonate	6420633	46	$C_{14}H_{23}Cl_3O_3$	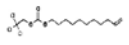
32.55	1.32	7, 9-Ditert-Butyl-1-Oxaspiro [4.5] Deca-6,9-Diene-2,8-Dione	545303	27	$C_{17}H_{24}O_3$	
37.11	3.11	Methyl (Z)-Octadec-6-Enoate	5362717	46	$C_{19}H_{36}O_2$	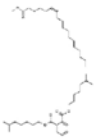
49.33	0.49	Bis (6-Methylheptyl) Benzene-1,2-Dicarboxylate	33934	58	$C_{24}H_{38}O_4$	
49.50	0.7287	1-Hydroxy-4-Methoxy-3,3-Dimethylindol-2-One	610113	52	$C_{11}H_{13}NO_3$	

Table 2. Secondary phytochemical compounds identified by GC-MS in methanolic extracts of *S. vulgare*

Peak RT	Area %	secondary compounds	CID	Qual	Molecular Formula	Chemical Structure
23.31	2.46	Pentadecane	23.31	2.46	Pentadecane	
23.72	2.73	2,4-Di-Tert-Butylphenol	7311	72	$C_{14}H_{22}O$	
24.38	1.44	Hexadecane	11006	86	$C_{16}H_{34}$	
28.21	3.88	3-Ethyl-5-(2-Ethylbutyl)Octadecane	292285	80	$C_{26}H_{54}$	
32.65	5.77	methyl hexadecanoate	8181	90	$C_{17}H_{34}O_2$	
27.99	2.25	Heptacosane	11636	64	$C_{27}H_{56}$	
25.75	2.56	3,7-Dimethylundecane	519387	53	$C_{13}H_{28}$	
29.14	1.83	Octacosane	12408	59	$C_{28}H_{58}$	
30.91	1.60	Hept-2-Ynal	549253	35	$C_7H_{10}O$	
35.93	1.91	1-(2-Cyclohexyliminocyclopentyl) Ethanone	610112	35	$C_{13}H_{21}NO$	
36.13	1.94	(E,7r,11r)-3,7,11,15 Tetramethylhexadec-2-En-1-Ol	5280435	49	$C_{20}H_{40}O$	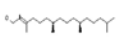
43.31	5.79	Dioctyl Benzene-1,2-Dicarboxylate	8346	50	$C_{17}H_{34}O_2$	

residues and binding sites within ETA include Glu ^{553}, His ^{440}, Tyr ^{481}, Tyr ^{470}, Glu ^{546}, and Arg ^{551} in domain III (Jørgensen et al., 2008; Carrol and Collier, 197) (Figure 4). Docking simulations were employed to predict the interaction sites of the ligands with protein targets and to assess the binding affinities of the small molecules (Odoemelam et al., 2022). All ligands successfully docked with ETA. The binding affinities, represented in kcal/mol, for the docked ligands, as shown in Table 3 and Table 4, ranged from 5.2 to 8.2 and 4.7 to 7.7 kcal/mol for the bioactive compounds derived from ethanolic and methanolic extracts, respectively (Table 1 and Table 2). The further molecular docking results displayed that the ligands engaged in significant hydrophobic interactions, hydrogen bonds, salt bridge formations, and, in certain instances, p–p stacking interactions. These findings suggested that the binding site predominantly consists of the hydrophobic amino acid (AA) residues (Table 3 and Table 4).

Figure 5 presents a schematic diagrams illustrating the Protein-Ligand Interactions as analyzed by LigPlot, specifically for selective ligands that exhibit high binding affinity and favourable interactions with the residues located at the active sites.

Results of the ADME studies

In this study, the SwissADME web tool was employed to assess the physicochemical properties, pharmacokinetics, and drug-likeness of some of the *S.vulgare* extract's compounds. The capacity of a drug to penetrate membranes for transport throughout the body is highly correlated with its physicochemical properties (Hernandez et al., 2024). The ligands (E2, E9, E13, E15, E16, M2, M10, M11, and M12) with high binding affinity and good interaction with active site residues were selected for the ADME study (Praveen et al., 2023). The findings of SwissADME, including physicochemical, pharmacokinetic, and drug-likeness properties of the selective ligands, are listed in Table 5. The basic physicochemical properties such as the molecular weights of the selected compounds ranged from 206.32 to 390.56 (g/mol). The lipophilicity value (LogP) for the selected compounds varied from 1.4 to 5.25. The ccalculated water solubility index displayed that all compounds were water-soluble,which was varied in solubility levels. According to the ADMET properties, all the compounds with the exception of M11, showed high gastrointestinal absorption, while the potential for Blood Brain Barrier (BBB) penetration was predicted for all the compounds except E15, M11, and M12. The computed drug-likeness properties indicated that compounds E2, M2, E13, E16, and M10 did not violate either of the two filters (Lipinski and Veber rules) applied. Conversely, the remaining compounds (E9, E15, M11, and M12) exhibited one violation of the drug-likeness filters. The synthetic accessibility scores for the compounds ranged from 1.43 to 4.35.

The graphical output produced by SwissADME consists of the BOILED egg plot (Figure 6) which illustrates the solubility properties of the selective metabolites derived from *S. vulgare.* The BOILED-Egg allows for intuitive evaluation of passive gastrointestinal absorption (HIA)

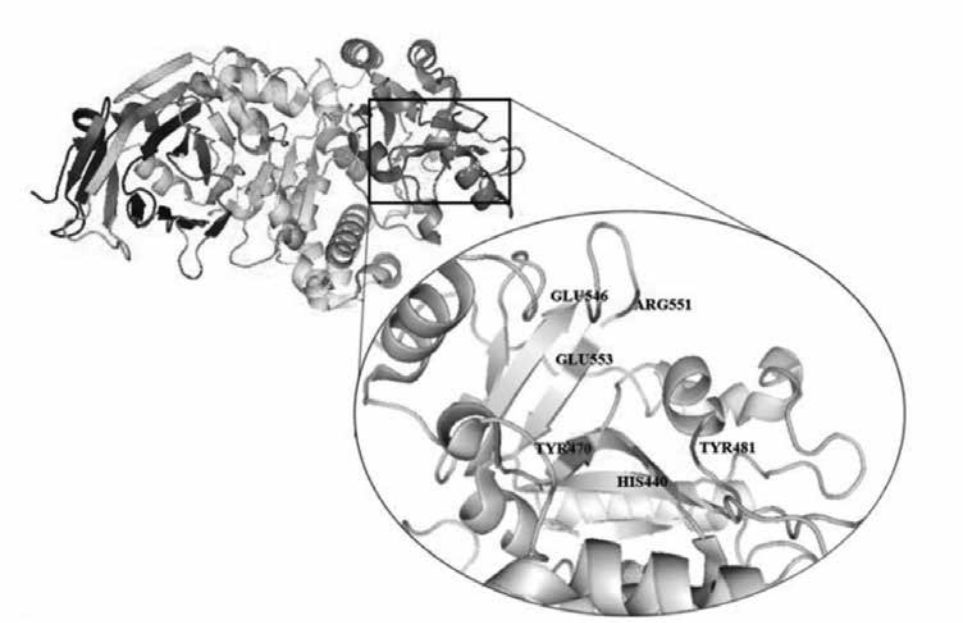

Fig. 4. The three-dimensional structure of 1IKQ with the binding site and its amino acids

Table 3. Molecular Docking Results of Secondary Phytochemical Compounds Identified By GC-MS in Ethanolic Extract of *S. Vulgare*

N	Ligand Name	Binding Affinity (Kcal/Mol)	Hydrophobic Interaction	Hydrogen Bond	Salt Bridge	Π-Stacking (Parallel)
E1	1-Iodotridecane	-5.4	440A:HIS, 441A:GLY, 470A:TYR, 471A:ILE, 472A:ALA, 477A:LEU, 478A: ALA, 481A:TYR, 553A: GLU			
E2	2,4-ditert-butylphenol	-7.7	439A:TYR, 440A:HIS, 441A:GLY, 470A:TYR, 471A:ILE, 472A:ALA, 477A:LEU, 478A:ALA, 481A:TYR, 553A:GLU, 554A:THR			440A:HIS, 481A:TYR
E3	3,5dimethyloctan-2-one	-5.4	440A:HIS, 441A:GLY, 470A:TYR, 471A:ILE, 472A:ALA, 477A:LEU, 478A: ALA, 481A:TYR, 546A:GLU, 553A: GLU, 554A:THR	441A:GLY		
E4	tridecan-3-yl 2-methoxyacetate	-5.9	440A:HIS, 441A:GLY, 442A:THR, 458A:ARG, 460A:GLN, 470A:TYR, 471A:ILE, 472A:ALA 477A:LEU, 478A: ALA, 481A:TYR, 553A: GLU		440A:HIS, 458A:ARG	
E5	Octadecane	-5.9	440A:HIS, 441A:GLY, 460A:GLN, 462A:LEU, 470A:TYR, 471A:ILE, 472A:ALA, 477A:LEU, 478A: ALA, 481A:TYR, 553A: GLU			481A:TYR
E6	ethyl hexadecanoate	-5.7	440A:HIS, 441A:GLY, 442A:THR, 458A:ARG, 469A:PHE, 470A:TYR, 471A:ILE, 472A:ALA, 477A:LEU, 478A: ALA, 481A:TYR, 553A: GLU, 558A:TRP		440A:HIS, 458A:ARG	481A:TYR
E7	9-Octylicosane	-6.6	440A:HIS, 441A:GLY, 442A:THR, 443A:PHE, 458A:ARG, 460A:GLN, 468A:GLY, 469A:PHE, 470A:TYR, 471A:ILE, 472A:ALA, 477A:LEU, 481A:TYR, 483A:GLN, 546A:GLU, 553A: GLU, 558A:TRP			
E8	Hentriacontane	-5.8	440A:HIS, 441A:GLY, 443A:PHE, 458A:ARG, 460A:GLN, 469A:PHE, 470A:TYR, 471A:ILE, 472A:ALA, 477A:LEU, 481A:TYR, 483A:GLN, 553A: GLU, 558A:TRP			
E9	2-[12-(oxiran-2-yl)dodecyl]oxirane	-7.2	439A:TYR, 440A:HIS, 458A:ARG, 460A:GLN, 462A:LEU, 470A:TYR, 471A:ILE, 481A:TYR, 558A:TRP	441A:GLY, 458A:ARG		481A:TYR
E10	4-Methyldocosane	-7.3	440A:HIS, 441A:GLY, 458A:ARG, 468A:GLY, 469A:PHE, 470A:TYR, 471A:ILE, 472A:ALA, 477A:LEU, 481A:TYR, 553A: GLU, 558A:TRP			
E11	(E)-1-methoxydodec-2-ene	-5.2	441A:GLY, 458A:ARG, 468A:GLY, 469A:PHE, 470A:TYR, 471A:ILE, 472A:ALA, 477A:LEU, 481A:TYR, 553A: GLU, 558A:TRP	460A:GLN		
E12	2,2,2-trichloroethyl undec-10-enyl carbonate	-6.3	441A:GLY, 442A:THR, 450A:ILE, 458A:ARG, 469A:PHE, 470A:TYR, 471A:ILE, 472A:ALA, 477A:LEU, 481A:TYR, 553A:GLU, 558A:TRP	440A:HIS		
E13	7,9-Ditert-Butyl-1-Oxaspiro[4.5]Deca-6,9-Diene-2,8-Dione	-8.2	440A:HIS, 441A:GLY, 442A:THR, 443A:PHE, 460A:GLN, 469A:PHE, 470A:TYR, 481A:TYR, 558A:TRP	458A:ARG	440A:HIS	
E14	Methyl (Z)-Octadec-6-Enoate	-6.2	440A:HIS, 441A:GLY, 460A:GLN, 470A:TYR, 471A:ILE, 472A:ALA, 477A:LEU, 481A:TYR, 546A:GLU, 553A:GLU,	460A:GLN	458A:ARG	
E15	Bis(6-Methylheptyl) Benzene-1,2-Dicarboxylate	-7.2	442A:THR, 460A:GLN, 462A:LEU, 468A:GLY, 469A:PHE, 470A:TYR, 471A:ILE, 472A:ALA, 477A:LEU, 481A:TYR, 553A:GLU, 558A:TRP	440A:HIS, 458A:ARG		
E16	1-Hydroxy-4-Methoxy-3,3-Dimethylindol-2-One	-7.1	440A:HIS, 470A:TYR, 471A:ILE, 472A:ALA, 477A:LEU, 481A:TYR, 553A:GLU	441A:GLY		481A:TYR

Table 4. Molecular Docking Results of Secondary Phytochemical Compounds Identified by GC-MS in Methanolic Extract of *S. Vulgare*

N	Ligand Name	Binding Affinity (Kcal/Mol)	Hydrophobic Interaction	Hydrogen Bond	Salt Bridge	Π-Stacking (Parallel)
M1	Pentadecane	-5.8	440A:HIS, 441A:GLY, 458A:ARG, 468A:GLY, 469A:PHE, 470A:TYR, 471A:ILE, 472A:ALA, 477A:LEU, 481A:TYR, 553A:GLU, 558A:TRP			
M2	2,4-Di-Tert-Butylphenol	-7.7	439A:TYR, 440A:HIS, 441A:GLY, 470A:TYR, 471A:ILE, 472A:ALA, 477A:LEU, 478A:ALA, 481A:TYR, 553A:GLU, 554A:THR			440A:HIS, 481A:TYR
M3	Hexadecane	-5.8	440A:HIS, 441A:GLY, 460A:GLN, 468A:GLY, 469A:PHE, 470A:TYR, 471A:ILE, 472A:ALA, 477A:LEU, 481A:TYR, 558A:TRP			
M4	3-Ethyl-5-(2-Ethylbutyl)Octadecane	-6	440A:HIS, 441A:GLY, 442A:THR, 458A:ARG, 460A:GLN, 462A:LEU, 468A:GLY, 469A:PHE, 470A:TYR, 481A:TYR, 558A:TRP			
M5	methyl hexadecanoate	-6.2	439A:TYR, 440A:HIS, 441A:GLY, 468A:GLY, 469A:PHE, 470A:TYR, 471A:ILE, 472A:ALA, 477A:LEU, 478A:ALA, 481A:TYR, 558A:TRP	460A:GLN	458A:ARG	
M6	Heptacosane	-5.9	439A:TYR, 440A:HIS, 441A:GLY, 443A:PHE, 458A:ARG, 460A:GLN, 462A:LEU, 469A:PHE, 470A:TYR, 471A:ILE, 472A:ALA, 477A:LEU, 478A:ALA, 481A:TYR, 553A:GLU, 558A:TRP			
M7	3,7-Dimethylundecane	-5.5	439A:TYR, 441A:GLY, 470A:TYR, 471A:ILE, 472A:ALA, 477A:LEU, 478A:ALA, 481A:TYR, 546A:GLU, 553A:GLU			
M8	Octacosane	-5.9	440A:HIS, 441A:GLY, 458A:ARG, 462A:LEU, 468A:GLY, 469A:PHE, 470A:TYR, 471A:ILE, 472A:ALA, 477A:LEU, 478A:ALA, 481A:TYR, 553A:GLU, 558A:TRP			
M9	Hept-2-Ynal	-4.7	439A:TYR, 440A:HIS, 470A:TYR, 471A:ILE, 472A:ALA, 477A:LEU, 478A:ALA, 481A:TYR, 546A:GLU, 553A:GLU	441A:GLY		
M10	1-(2-Cyclohexyliminocyclopentyl)Ethanone	-6.9	439A:TYR, 440A:HIS, 441A:GLY, 470A:TYR, 471A:ILE, 472A:ALA, 477A:LEU, 478A:ALA, 553A:GLU	470A:TYR		
M11	(E,7r,11r)-3,7,11,15 Tetramethylhexadec-2-En-1-Ol	-6.4	439A:TYR, 440A:HIS, 441A:GLY, 468A:GLY, 469A:PHE, 470A:TYR, 471A:ILE, 472A:ALA, 477A:LEU, 478A:ALA, 481A:TYR, 553A:GLU	470A:TYR		
M12	Dioctyl Benzene-1,2-Dicarboxylate	-6.6	439A:TYR, 440A:HIS, 441A:GLY, 458A:ARG, 471A:ILE, 472A:ALA, 477A:LEU, 478A:ALA, 481A:TYR, 483A:GLN, 485A:GLN, 546A:GLU, 553A:GLU	460A:GLN, 470A:TYR	440A:HIS	

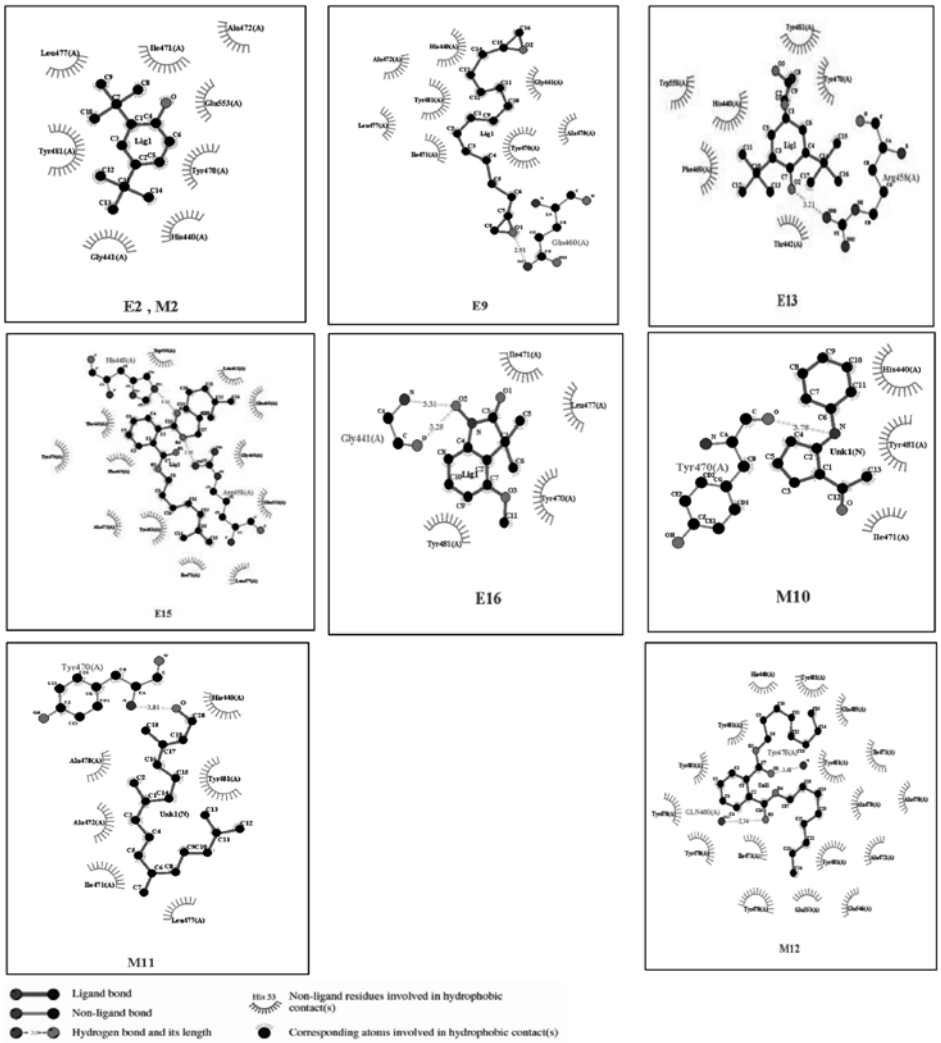

Fig. 5. Schematic Diagram of Protein-Ligand Interactions for selective ligands using the LigPlot

Table 5. Physico Chemical, Pharmacokinetic, and Drug Likeness Properties of the top binding Ligands

Properties	E2, M2	E9	E13	E15	E16	M10	M11	M12
Formula	$C_{14}H_{22}O$	$C_{16}H_{30}O_2$	$C_{17}H_{24}O_3$	$C_{24}H_{38}O_4$	$C_{11}H_{13}NO_3$	$C_{13}H_{21}NO$	$C_{20}H_{40}O$	$C_{24}H_{38}O_4$
MV(g/mol)	206.32	254.41	276.37	390.56	207.23	207.31	296.53	390.56
Num. heavy atoms	15	18	20	28	15	15	21	28
Num. rotatable bonds	2	13	2	16	1	2	13	18
Num. H-bond acceptors	1	2	3	4	3	2	1	4
Num. H-bond donors	1	0	0	0	1	0	1	0
Molar Refractivity	67.01	76.97	79.66	116.3	58.55	64.26	98.94	116.3
TPSA (Å2)	20.23	25.06	43.37	52.6	49.77	29.43	20.23	52.6
Log $P_{o/w}$ (MLOG)	3.87	3.13	2.87	5.24	1.4	2.11	5.25	5.24
Solubility	Moderately soluble	Soluble	Soluble	Poorly soluble	Soluble	Soluble	Moderately soluble	Poorly soluble
GI absorption	High	High	High	High	High	High	Low	High
BBB permeability	Yes	Yes	Yes	No	Yes	Yes	No	No
Violation of Lipinski rule	0	0	0	1	0	0	1	1
Violation of Veber rule	0	1	0	1	0	0	1	1
Synthetic accessibility	1.43	3.09	4.35	3.41	2.22	3.19	4.3	3.41

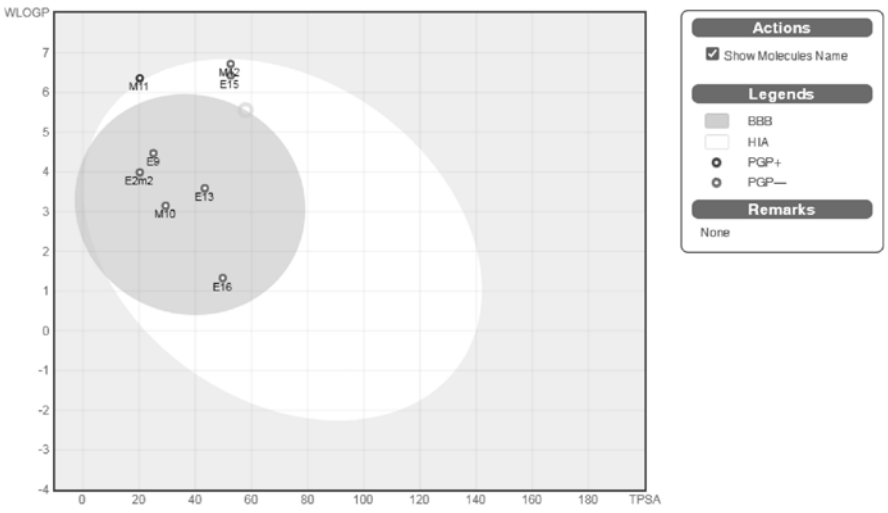

Fig. 6. BOILED-Egg plot of the top binding Ligands obtained from SwissADME

and brain penetration (BBB) in function of the position of the molecules in the WLOGP-versus-TPSA referential. The white region is high probability of passive absorption by the gastrointestinal tract, and the yellow area (yolk) is for high probability of brain penetration. In addition, the points are colored in blue if predicted as actively effluxes by P-gp (PGP+) and in red if predicted as non-substrate of P-gp (PGP−) (Daina et al., 2017). The ligands E2, E9, E13, E16, M2, and M10 are positioned within the yellow zone, while M12, E15 are located in the white zone, and M11 is situated in the gray zone, so it is predicted as not absorbed and not brain penetrant (outside the Egg), M12 and E15 are predicted well-absorbed but not accessing the brain (in the white) and

PGP− (red dot), and E2, E9, E13, E16, M2 and M10 are predicted as brain-penetrant (in the yolk) and not subject to active efflux (red dot).

Discussion

Numerous studies have reported that various algal extracts possess significant potential as a beneficial source of novel bioactive compounds with pharmaceutical relevance. These extracts have revealed antibacterial properties against various a range of pathogenic strains (El-Sapagh et al., 2023). The research conducted by suggests the potential of algal extracts as agents against both bacterial infections and biofilm formation, particularly in the context of drug-resistant P. aeruginosa. Notable compounds such as phytol, bromophenol, and dihydroxybenzaldehyde have been identified as contributors to these activities. Furthermore, an analysis performed using the SwissDock Web server indicated promising physicochemical properties of the algal extracts, suggesting their potential application as antimicrobial agents (El-Sapagh et al., 2023).

In the present study, the GC-MS analysis of *S. vulgare* extracts showed the presence of 28 compounds, which were subsequently docked as ligands to the ETA of *P. aeruginosa* to evaluate their antibacterial ability. For instance, a study by Rajkumar et al. (2018) highlighted that the ethanolic extract of *Sargassum polycystem* (Rajkumar et al., 2018) showed significant activity against *P. aerugionsa*. In *P. aeruginosa*, ETA, indeces cellular toxicity through the ADP ribosylation of translation elongation factor 2, follow leading to enzyme cleavage activity and the binding of cell surface receptors, which can result in toxicity in infected cells, thereby underscoring the importance of this target. Notably, compounds such as 1, 2 benzenedicarboxylic-dibutyl ester, 1, 3 docosenamide, and 3, 5 diaminodeoxymethoxy showed considerable antibacterial activity against ETA (Rajkumar et al., 2018). Further moreanother study reported that brown algae serve as a rich source of bioactive molecules with significant biological activities. The chemical compounds of *Sargassum* sp exhibited favorable drug-ability, bioavailability, and pharmacokinetic properties along with anti-biofilm efficacy and antibacterial activity against antibiotic-resistant strains of *Staphylococcus* (Alreshidi et al., 2023).

In the current study examining 28 phytochemical compounds of *S. vulgare*, the 28 compounds of *S. vulgare*, 7, 9-Ditert-Butyl-1-Oxaspiro [4.5] Deca-6,9-Diene-2,8-Dione (E13) and 2,4-ditert-butylphenol (E2, M2) showed the most significant binding affinity with ETA, So this makes them promising candidate for pharmacokinetic development targeting ETA. It is important to note that, in addition to binding affinity, other factors also contribute to this assessment. Weak intermolecular interactions, such as hydrogen bonding and hydrophobic interactions, play a significant role in stabilizing a ligand at the interface of a protein structure (Patil et al., 2010). Hydrogen bonds (HB) are particularly significant biological systems, influencing the binding affinity and selectivity of protein-ligand interactions (Madushanka et al., 2023). The docking

interactions results presented in Tables 3 and 4 indicate that ETA formed Hydrogen bonds with seven compounds from the ethanolic extract and five compounds of methanolic extract, involving amino acid residues such as HIS [440], GLY[441], ARG[458], GLN[460], and TYR[470]. previous studies have reported that hydrophobic interactions can enhance the binding affinity at ligand-receptor interfaces in drug designing (Patil et al., 2010). This study also observed a substantial number of hydrophobic interactions between metabolites and ETA, as detailed in Tables 3 and 4. The ligands E2, E9, E13, E15, E16, M2, M10, M11, and M12 exhibited strong binding affinity and favorable interactions, including hydrophobic interactions, hydrogen bond, salt bridge, and Π-Stacking, with the active site residues (Glu [553], His [440], Tyr [481], Tyr [470], Glu [546] and Arg [551]) of ETA.

For a molecule to function effectively as a drug, it must reach its intended target within the body at a sufficient concentration and remain in a bioactive state long enough for the anticipated biological processes to take place (Daina et al., 2017; Milusheva et al., 2023). Lipinski proposed several criteria for determining the solubility and permeability of a compound to be considered a viable drug candidate, comprising the molecular mass should be less than 500 Dalton; the hydrogen bond donor should be less than 5, hydrogen bond acceptor should be less than 10, Mlog P should be less than 4.15 (Lipinski, Lombardo, Dominy, & Feeney, 1997; Praveen et al., 2023). As indicated in Table 5, all selective ligands, with the except of three (E15, M11, and M12), adhere to these criteria, with the sole infraction being the MLog P value, which exceeds 4.15. A single deviation from the Lipinski rule is permissible (Benet et al., 2016; Praveen et al., 2023)thereby, allowing all leading ligands to be considered as potential drug candidates. Based on Veber's rule, the rotatable bonds should be fewer than 10, and the polar surface area should be equal to or less than 140 Å to ensure a high likelihood of favorable oral bioavailability (Veber et al., 2002). Out of the nine top binding metabolites, five (E2, M2, E13, E16, and M10) adhere to Veber's rule. Furthermore, the SwissADME Synthetic Accessibility (SA) Score is primarily based on the premise that the prevalence of molecular fragments in 'readily' obtainable compounds is indicative of their synthetic feasibility. The SA score ranges values from 1 (indicating ease to synthesis) to 10 (indicating difficulty in synthesis) (Skoraczyński et al., 2023), suggesting that these metabolites can be synthesized with relative ease, as their synthetic accessibility scores are all below 5. In the BOILED-Egg plot, the compounds capable of traversing the Blood Brain Barrier are indicated in the yellow zone. The white zone signifies those compounds that can be absorbed by the human gastrointestinal tract (HIA). Conversely, the grey zone denotes compounds that are unable to cross the BBB nor be absorbed by the HIA (Praveen et al., 2023). As illustrated in Figure 6, compounds E2, E9, E13, E16, M2, and M10 are located in the yellow zone, indicating their ability to permeate through the Blood Brain Barrier. Compounds M12 and E15 are found in the white zone, suggesting they can be absorbed through the gastrointestinal tract. In contrast,

compound M11 is situated in the gray zone, indicating that this metabolite can neither cross the BBB nor be absorbed in the HIA. Ultimately, the ligands listed in Table 5 can bind to the active sites of ETA, therebinhibitingthe activities of the ADP-ribosyl transferase (domain III). Based on to the findings from ADME and BOILED-Egg plot analysis, the compounds M12 and E15 demonstrate superior human intestinal absorption. Furthermore, neither of these compounds is capable of penetrating the blood-brain barrier which is desirable given that the brain is not intended targeted. Consequently, these compounds appear to be promising candidate for drug development due to their effective drug-likeness properties.

Recently, numerous bioactive compounds isolated from *Sargassum. sp* have been studied for their potential applications in pharmaceuticals (Cho et al., 2022). This research highlights the promise of marine natural products in producing metabolites with beneficial biological activities and emphasizes the significance of in silico methodologies in facilitating drug discovery. In this study, metabolites extracted from *S. vulgare* were employed to inhibit ADP-ribosyl transferase of ETA through molecular docking and SwiissADME analysis, aiming to evaluate the antibacterial efficacy of these metabolitesThe findings suggested that the compounds M12 (Dioctyl Benzene-1, 2-Dicarboxylate) and E15 (Bis (6-Methylheptyl) Benzene-1, 2-Dicarboxylate) from *S. vulgare* may serve as effective antibacterial agent against *P. aeruginosa*. The results of this research could aid in the design of novel molecules exhibiting significant biological activity with reduced side effects. However, it is important to note that these predictions are based onin-silico methods, which are not devoid of challenges and limitations inherent in predictive tools. Therefore, to confirm this prediction, further in vitro and in vivo studies are essential to confirm the antibacterial properties derived from *S. vulgare*.

Acknowledgement

The authors express their gratitude to Khorramshahr Marine Science and Technology University's Department of Marine Biology for providing us with this invaluable scientific work opportunity and the facilities needed to conduct research

References

Abu Ahmed SE., Deyab MA., El-Ashry FS., El-Adl MF. (2021). Qualitative and Quantitative Phytochemical Composition of *Sargassum Vulgare* at Hurghada Red Sea Coast-Egypt. Scientific Journal for Damietta Faculty of Science. 11 (1): 10-19. DOI:10.21608/SJDFS.2021.195585.

Adetayo MO and Anyasor GS. (2022). In Silico Investigation of Gastroprotective Compounds from n-Butanol Fraction of *Costus igneus* on Antiulcer Druggable Targets. The FASEB Journal. 36. DOI:10.1096/fasebj.2022.36.S1.R3085.

Alreshidi M., Badraoui R., Adnan M., Patel M., Alotaibi A., Saeed M., Ghandourah M., Al-Motair KA., Arif IA., Albulaihed Y., Snoussi M. (2023). Phytochemical

profiling, antibacterial, and antibiofilm activities of *Sargassum* sp.(brown algae) from the Red Sea: ADMET prediction and molecular docking analysis. Algal Research. 69: 102912. DOI: 10.1096/fasebj.2022.36.S1.R3085.

Arguelles ED., Monsalud RG., Sapin AB. (2019). Chemical composition and in vitro antioxidant and antibacterial activities of *Sargassum vulgare* C. Agardh from Lobo, Batangas, Philippines. Journal of the International Society for Southeast Asian Agriculture Sciences. 25: 112-122. DOI: www.ukdr.uplb.edu.ph/journal-articles/700.

Benet LZ., Hosey CM., Ursu O., Oprea TI. (2016). BDDCS, the Rule of 5 and drugability. Advanced Drug Delivery Reviews. 101: 89-98. DOI:10.1016/j.addr.2016.05.007.

Bultum LE., Tolossa GB., Lee D. (2022). Combining empirical knowledge, in silico molecular docking and ADMET profiling to identify therapeutic phytochemicals from *Brucea antidysentrica* for acute myeloid leukemia. Plos One. 17 (7): e0270050. DOI: 10.1371/journal.pone.0270050.

Carroll SF and Collier RJ. (1987). Active site of *Pseudomonas aeruginosa* exotoxin A. Glutamic acid 553 is photolabeled by NAD and shows functional homology with glutamic acid 148 of diphtheria toxin. Journal of Biological Chemistry. 262 (18): 8707-8711. DOI:10.1016/S0021-9258(18)47472-8.

Cho CH., Lu YA., Kim MY., Jeon YJ,. Lee SH. (2022). Therapeutic potential of seaweed-derived bioactive compounds for cardiovascular disease treatment. Applied Sciences. 12 (3): 1025. DOIoi:10.3390/app12031025.

Daina A., Michielin O., Zoete V. (2017). SwissADME: a free web tool to evaluate pharmacokinetics, drug-likeness, and medicinal chemistry friendliness of small molecules. Scientific reports. 7 (1): 42717. DOI:10.1038/srep42717.

El-Sapagh S., El-Shenody R., Pereira L., Elshobary M. (2023). Unveiling the potential of algal extracts as promising antibacterial and antibiofilm agents against multidrug-resistant *Pseudomonas Aeruginosa*: in vitro and in silico studies including molecular docking. Plants. 12 (18): 3324. DOI:10.3390/plants12183324.

Faisal al-hashdy D., El-Shaibany AM., Raweh SM., Humaid AA., El–Aasser MM. (2022). Preliminary phytochemical screening for various secondary metabolites, quantitative and qualitative analysis of Yemeni brown seaweed *Sargassum vulgare*. GSC Biological and Pharmaceutical Sciences. 20 (1): 298-313. DOI:10.30574/gscbps.2022.20.1.0294.

Gade AC., Murahari M., Pavadai P., Kumar MS. (2023). Virtual Screening of a Marine Natural Product database for In Silico identification of a potential Acetylcholinesterase inhibitor. Life, 13 (6): 1298.DOI:10.3390/life13061298.

Garg S., Anand A., Lamba Y., Roy A. (2020). Molecular docking analysis of selected phytochemicals against SARS-CoV-2 Mpro receptor. Vegetos. 33 (4): 766-781. DOI: 10.1007/s42535-020-00162-1.

Guiry MD., Guiry GM., Morrison L., Rindi

F, Miranda SV., Mathieson AC., Parker BC., Langangen A., John DM., Bárbara I., Carter CF. (2014). AlgaeBase: an on-line resource for algae. Cryptogamie, Algologie. 35(2): 105-115. DOI:10.7872/crya.v35.iss2.2014.105.

Haddad M., Gaudreault R., Sasseville G., Nguyen PT., Wiebe H., Van De Ven T., Bourgault S., Mousseau N., Ramassamy C. (2022). Molecular interactions of tannic acid with proteins associated with SARS-CoV-2 infectivity. International journal of molecular sciences. 23(5): 2643. DOI:10.3390/ijms23052643.

Hernandez RD., Genio FA., Casanova JR., Conato MT., Paderes MC. (2024). Antiproliferative Activities and SwissADME Predictions of Physicochemical Properties of Carbonyl Group-Modified Rotenone Analogues. Chemistry Open. 13 (1): e202300087. DOI:10.1002/open.202300087.

Jørgensen R., Wang Y., Visschedyk D., Merrill AR. (2008). The nature and character of the transition state for the ADP-ribosyltransferase reaction. EMBO Reports. 9 (8): 802-809. DOI:10.1038/embor.2008.90.

Kothandan R., Rajan CA., Arjun J., Raj RR., Syed S. (2021). Virtual screening of phytochemical compounds as potential inhibitors against SARS-CoV-2 infection. Beni-Suef University Journal of basic and applied sciences. 10 (1): 1-7. DOI:10.1186/s43088-021-00095-x.

Liao W., Huang L., Han S., Hu D., Xu Y., Liu M., Yu Q., Huang S., Wei D., Li P. (2022). Review of medicinal plants and active pharmaceutical ingredients against aquatic pathogenic viruses. Viruses. 14(6): 1281. DOI:10.3390/v14061281.

Lipinski CA., Lombardo F., Dominy BW., Feeney PJ.. (1997). Experimental and computational approaches to estimate solubility and permeability in drug discovery and development settings. Advanced Drug Delivery Reviews. 23 (1-3): 3-25. DOI:10.1016/S0169-409X(96)00423-1.

Liu PV. (1974). Extracellular toxins of *Pseudomonas aeruginosa*. Journal of Infectious Diseases. 130 (Supplement): S94-S99. DOI:10.1093/infdis/130.Supplement.S94.

Madushanka A., Moura Jr RT., Verma N., Kraka E. (2023). Quantum mechanical assessment of protein–ligand hydrogen bond strength patterns: insights from semiempirical tight-binding and local vibrational mode theory. International Journal of Molecular Sciences. 24 (7): 6311. DOI: 10.3390/ijms24076311.

Miandad K., Ullah A., Bashir K., Khan S, Abideen SA., Shaker B., Alharbi M., Alshammari A., Ali M., Haleem A., Ahmad S. (2022). Virtual Screening of *Artemisia annua* phytochemicals as Potential Inhibitors of SARS-CoV-2 main protease nzyme. Molecules. 27(22): 8103. DOI:10.3390/molecules27228103.

Milusheva M., Gledacheva V., Stefanova I., Nikolova S. (2023). 1-(2-Chlorophenyl)-6, 7-dimethoxy-3-methyl-3, 4-dihydroisoquinoline. Molbank. 2023 (2): M1608. DOI:10.3390/M1608.

Mishra A. AND Dey S. (2019). Molecular docking studies of a cyclic octapeptide-

cyclosaplin from sandalwood. Biomolecules. 9 (11): 740. DOI: 10.3390/biom9110740.

Mohammed HA., Almahmoud SA., Arfeen M., Srivastava A., El-Readi MZ., Ragab EA., Shehata SM., Mohammed SA., Mostafa EM., El-khawaga HA., Khan RA. (2022). Phytochemical profiling, molecular docking, and in vitro anti-hepatocellular carcinoid bioactivity of Suaeda vermiculata extracts. Arabian Journal of Chemistry. 15 (7): 103950. DOI:10.1016/j.arabjc.2022.103950.

Odoemelam CS., Hunter E., Simms J., Ahmad Z., Chang MW., Percival B., Williams IH., Molinari M., Kamerlin SC., Wilson PB. (2022). In Silico Ligand Docking Approaches to Characterise the Binding of Known Allosteric Modulators to the Glucagon-Like Peptide 1 Receptor and Prediction of ADME/Tox Properties. Applied Biosciences. 1(2): 143-162. DOI:10.3390/applbiosci1020010.

Patil R, Das S, Stanley A, Yadav L, Sudhakar A, Varma AK. (2010). Optimized hydrophobic interactions and hydrogen bonding at the target-ligand interface lead the pathways of drug-designing. PLoS One. 5 (8): e12029. Doi:10.1371/journal.pone.0012029.

Prasanth R and Suresh Kumar P. (2020). Molecular docking and statistical assessment of macroalgae Halimeda species against marine macro fouler *Mytilus galvoprovinces* (4CN8). Int. Journal Pharmaceutical Sciences Review Research. 60: 40-47.

Praveen AS., Vinitha S., Vinayalekshmi VS., Ramya P., Vanavil B. (2023). Seaweed metabolites for targeting pel polysaccharide biosynthesis in *Pseudomonas aeruginosa*–A novel strategy for biofilm control. Current Trends in Biotechnology and Pharmacy. 17 (3B): 1316-1326. DOI:10.5530/ctbp.2023.3s.66.

Rajkumar G., Bhavan PS., Suganya M., Srinivasan V., Karthik M., Udayasuriyan R. (2018). Phytochemical characterization of marine macro alga *Sargassum polycystem*, molecular docking, and in vitro anti-bacterial activity against *Psuedomonas aeruginosa*. International Biological and Biomedical Journal. 4 (1): 35-47. DOI:ibbj.org/article-1-160-en.html.

Silva A., Silva SA., Carpena M., Garcia-Oliveira P., Gullón P., Barroso MF., Prieto MA., Simal-Gandara J. (2020). Macroalgae as a source of valuable antimicrobial compounds: Extraction and applications. Antibiotics. 9 (10): 642. DOI: 10.3390/antibiotics9100642.

Skoraczyński G, Kitlas M, Miasojedow B, Gambin A. (2023). Critical assessment of synthetic accessibility scores in computer-assisted synthesis planning. Journal of Cheminformatics. 15(1): 6. DOI:10.1186/s13321-023-00678-z.

Teibo JO., Bello SA., Adebisi OA., Olugbami JO., Ayandeyi TK. (2021). Anti-diabetic drug discovery using bioactive compounds: Molecular docking insights. GSC Biological and Pharmaceutical Sciences. 14(3): 175-178. DOI:10.30574/gscbps.2021.14.3.0048.

Veber DF., Johnson SR., Cheng HY., Smith BR., Ward KW., Kopple KD. (2002).

Molecular properties that influence the oral bioavailability of drug candidates. Journal of Medicinal Chemistry. 45(12): 2615-2623. DOI:10.1021/jm020017n.

Wedekind JE., Trame CB., Dorywalska M., Koehl P., Raschke TM, McKee M, FitzGerald D., Collier RJ., McKay DB. (2001). Refined crystallographic structure of Pseudomonas aeruginosa exotoxin A and its implications for the molecular mechanism of toxicity. Journal of Molecular Biology. 314 (4): 823-837. DOI:10.1006/jmbi.2001.5195.